PIER M

A Focused Circular Array with Variable Focal Length

Khalil H. Sayidmarie* and Mohammad Z. Mohammad Fwzi

Department of Communication Engineering, College of Electronics Engineering, Ninevah University, Mosul, Iraq

ABSTRACT: Focused arrays are attracting increased interest because of their wide range of applications. Focusing the antenna's radiation in the near field requires proper phase distribution of the array elements that must be fed through many phase shifters. This work presents a design idea for a focused circular array antenna, whose focal distance can be varied by only a single variable phase shifter. The idea is implemented on a dual ring circular array having a six-wavelength diameter and focused at five wavelengths by using a single fixed phase shifter. Theoretical analysis and computer simulations of a sample design using MATLAB and CST Microwave Studio show that a phase change of 0.9π leads to a four wavelength change in the focal distance. A formula for the estimation of the depth of field DOF is derived. The proposed array offers a simple method to vary the focal length continuously by a single variable phase shifter. This idea can be utilized in hyperthermia, RFID, and imaging applications, where the position of the focal spot needs to be moved along the normal to the array.

1. INTRODUCTION

One important application of antenna arrays is to concentrate the electromagnetic field in a certain volume near the antenna. Such antennas are referred to as focused arrays, in which the contributions of the entire antenna's elements arrive with the same phase at the focal spot, hence, they add constructively, while they combine destructively elsewhere. Focused arrays have found an increased interest in a wide range of applications [1, 2]. The focused electromagnetic field has been utilized for non-contact sensing in industrial inspection [3] and ground imaging radar [4], where the reflection of the localized field indicates a change in the reflecting medium. The focused electromagnetic field also means depositing energy at the focal region, thus elevating the temperature of a lossy medium. This phenomenon has been widely utilized in medical applications, especially in treating cancer by focusing the radiated field in the tumor [5–7], as well as in agricultural applications for weed control [8].

To implement focusing, phased arrays were found favorable due to their ability to offer more degrees of freedom and flexibility than single antennas. The array parameters, like geometry or layout of the elements, size, phase, and amplitude excitations of the array elements, have been utilized in various designs of the focused arrays. In [9], the performances of three array geometries for the focusing of the radiated field at a specific point in the near region of an array were compared. The elements in these arrays were placed to form a cross, a rectangular ring, and the conventional rectangular lattice. In the search for array geometries that can offer better focusing properties, six different array configurations were investigated in [10]. The array elements were placed on a square lattice, square lattice with interlaced element, square ring, cross, and letter (X) shape, as well as placing the elements on a square ring and diagonals. The six

array configurations were simulated assuming the same overall size, and the obtained characteristics were compared. The features of concern were field distribution around the focus, the lateral size of the focal spot, the depth of field (DOF) or the axial width of the focus, the maximum field at the focal point, and the level of the side lobes. A printed array comprising 16×16 dual-polarized elements, which were focused in the near field region, was presented in [11]. The array was designed to operate at 12 GHz and showed two independent focal spots generated by two feed networks.

There are two main geometries of the planar phased arrays, namely rectangular and circular arrays. In rectangular arrays, phase excitations of the elements have to be precisely determined to achieve an optimum focal spot. In near field microwave power transmission, for example, the transmitting array has to be focused, and the elements should also have amplitude tapering to achieve maximum beam collection efficiency. Therefore, the feeding network should be designed to offer various ratios of power division, which complicates and increases the cost of the feed network. In [12], the amplitude tapering of the 8×8 elements was performed in four levels (1, 0.5, 0.25, and 0.125) to simplify the feed network by using 3 dB dividers. However, adjusting the phases of the array elements required 4×4 phase shifters, which is an added complexity to the feed network.

The second form of the focused arrays is circular shape, where the array elements are placed in circles. Depending on the application, the focal spot can be either placed on the plane of the circular ring array or along the normal axis of the array plane. The first geometry was used in the array presented in [13], where the elements were positioned on a semicircle, and the focus was situated at the center of the circular arc. In alternative designs, the elements are placed on the whole circle as in [7], where a 16-element array was used to focus the radiation for thermotherapy, and in [14] the 16 array elements were

* Corresponding author: Khalil Hassan Sayidmarie (kh.sayidmarie@uninevah.edu.iq).

placed on the six sides of a hexagon. The focal point in these works is placed on the array plane.

The circular deployment of the elements was developed to a cylindrical configuration, where the elements are placed on the surface of a cylinder and arranged in the form of parallel rings. In [15], a hyperthermic applicator for cancer treatment consisting of ultra-wideband (UWB) microstrip elements placed on three parallel rings was presented. A comparison of the performances of single, double, and three layer configurations of the cylindrical arrays was published in [16]. In these configurations, there is no need for phase shifters in the feed network of the array elements if the desired focal spot is at the center of the array. However, by using phase shifters on each array element, the position of the focus can be moved to any point in the array plane as demonstrated in [7, 16].

In many applications, the focal spot is required to be in front of the focused array, as in radio frequency identification (RFID) and microwave imaging. A simple circular array consisting of two rings and a single phase shifter was proposed in [17]. The array radius was 50 cm, and the array was focused at a normal distance of 100 cm from the array plan. The 2-ring designed array was then developed into a 3-ring array comprising two phase shifters to achieve a smaller focal spot [18]. A focused circular array antenna operating at 2.45 GHz and employing 16 elements placed on two circles was reported in [19]. The elements were rectangular dielectric resonators fed by coaxial feeders. By adjusting the radii of the circles, the focal distance can be controlled. Thus, one has to redesign the array, by changing the outer radius for example to change the focal length of the array.

In a recent paper [20], we proposed a focused circular array comprising elements arranged on two concentric rings. The radius of the outer ring was determined such that the distances between the elements on this ring and the focal point differed by one wavelength from those for the elements on the inner ring. Such an arrangement leads to a constructive addition of the electric fields radiated by the elements at the focus, and consequently, no phase shifter is required. Therefore, only $M \times N/4$ phase shifters are needed in comparison with the case of the conventional $M \times N$ rectangular focused array. Moreover, the outer and inner rings are supplied with equal power, and the elements on each ring have uniform excitations in amplitude and phase thus simplifying the feed network [20]. In the search to reduce the feed network's complexity and to mitigate the need for phase shifters, a Ka-band, multilayer, near-field-focused substrate integrated array antenna was presented in [21]. The 8×8 element square array employed circular waveguides drilled in a thick conducting layer so that the holes operate as both phase shifters and radiating elements, thus separate phase shifters are not needed. By changing the thickness of the conducting layer, the same antenna can be adjusted to change its focal point, which means that a mechanical change is required to vary the focal point.

In this contribution, the design presented in [20] is developed to offer a variable focal length by adding a single variable phase shifter, while at the same time placing no condition on the radii of the rings. The variation of the focal length is achieved by feeding the elements of the inner ring through a single variable phase shifter that compensates the path difference of the two rings and yields focusing at a certain distance from the array. The proposed design offers flexibility and easy implementation, as it offers an electronic means to vary the focal distance in contrast to the designs presented in [19] and [21] where one of the array dimensions has to be changed.

The rest of the paper is structured as follows. Section 1 presents an introduction and survey, while the proposed circular array is analyzed in Section 2. Section 3 presents the results of the computer simulations performed in MATLAB and verified by other simulations performed with CST Microwave Studio Suite on the proposed focused array. In Section 4, the depth of field DOF is analyzed, and a formula is derived for the estimation of the DOF, while in Section 5, the lateral distribution of the radiated power density is presented. The drawn conclusions are listed in Section 6.

2. ANALYSIS OF THE PROPOSED CIRCULAR FOCUSED ARRAY

Circle array is one of the main shapes adopted in array design, where the elements are placed in concentric circles. Such a configuration offers circular symmetry that is utilized here to ease the design of the array. The proposed antenna comprises two concentric rings, having an inner radius of a and an outer radius of b as shown in Fig. 1. If the focal region is at distance F from the array plane and located at the point $P(0, 0, F)$, then the distances R_1 and R_2 from the focal point to the elements on the inner ring and outer ring respectively are:

$$R_1 = \sqrt{F^2 + a^2} \tag{1}$$

$$R_2 = \sqrt{F^2 + b^2} \tag{2}$$

$$\Delta R = R_2 - R_1 = \sqrt{F^2 + b^2} - \sqrt{F^2 + a^2} \tag{3}$$

where ΔR is the difference in the path lengths from the two rings to the focus at the point $P(0, 0, F)$. Suppose that there are M isotropic elements in the inner ring and N isotropic elements in the outer ring, and then the total field at any point on the Z-axis due to the inner ring E_i and due to outer ring E_o can be given by:

$$E_i(0, 0, z) = \sum_{m=1}^{M} E1 e^{-jkR1} = \frac{ME1}{R1} e^{-jkR1} \tag{4}$$

$$E_o(0, 0, z) = \sum_{n=1}^{N} E2 e^{-jkR2} = \frac{NE2}{R2} e^{-jkR2} \tag{5}$$

where k is the phase constant ($k = 2\pi/\lambda$), and λ is the wavelength. In general, the numbers of the elements on the two rings are not equal ($M \neq N$), and in the proposed array the magnitudes of the fields $|E_i(0, 0, F)|$ and $|E_o(0, 0, F)|$ at the focal point are set equal. The excitations of the elements on the ring that holds the smaller number of elements have to set by the following relation:
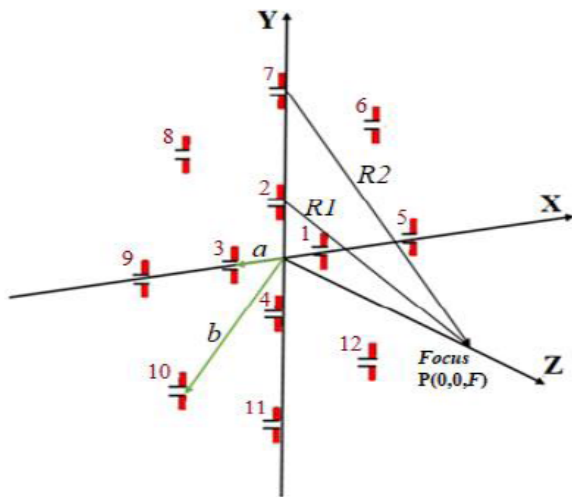
$$\frac{ME1}{R1} = \frac{NE2}{R2} = E \tag{6}$$

FIGURE 1. The geometry of the proposed focused array of M and N elements on the inner and outer rings respectively, positioned on the XY-plane.

FIGURE 2. Schematic of the feed network showing eleven 3 dB dividers, and a single variable phase shifter.

Thus, the elements on the inner ring should have excitations given by:

$$E1 = \frac{NR2}{MR1} E2 \qquad (7)$$

The geometry in Fig. 1 shows that the elements placed on the outer ring are farther to the focus than those on the inner ring. To achieve a focus, the electric fields radiated by the elements of the two rings must arrive in phase at the focal point. Therefore, the elements on the inner ring should be delayed by a certain path length q, then the sum of all the contributions along the Z-axis will be:

$$Et = \frac{ME1}{R1} e^{-jkR1} e^{-jkq} + \frac{NE2}{R2} e^{-jkR2} \qquad (8)$$

After adjusting the magnitudes of the excitations $E1$ and $E2$ according to Eqs. (6) and (7), the total electric field can be expressed as:

$$E_t = E * e^{-jk(R_1+q)}[1 + e^{-jk(R_2-R_1)} e^{jkq}] \qquad (9)$$

It can be shown that the total electric field at the observation point $P(0,0,z)$ attains a maximum value of

$$|E_t|_{\max} = 2E, \qquad (10a)$$

$$\text{when } R_2 R_1 = \Delta R = q, \qquad (10b)$$

Hence, the constructive addition is achieved at the focus (the point $P(0,0,F)$), and the above equation is a condition for focusing. As the above conditions (Eqs. (6), (7), and (10b)) have accounted for the phase shift and $1/R$ factor, Eq. (10a) represents the global maximum. On the other hand, when the contributions of the two rings are out of phase, they lead to a null, whose depth increases sharply as the compensation for the $1/R$ factor is implemented. For any other observation point
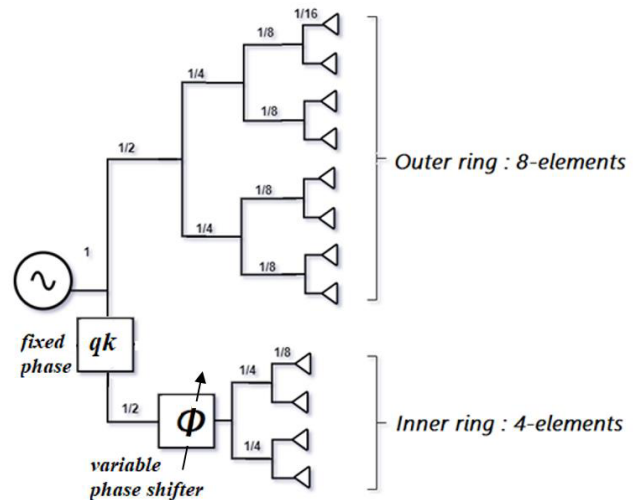
$P(0,0,z)$ where $z \neq F$, the path difference $\Delta R2$ is given by:

$$\Delta R2 = \sqrt{z^2 + b^2} - \sqrt{z^2 + a^2} \neq \sqrt{F^2 + b^2} - \sqrt{F^2 + a^2} \qquad (11)$$

Thus the total field is:

$$E_t(0,0,z) < 2E$$

Therefore, the contributions of all the elements on the two rings can be added to form a maximum (achieving a focus) when the elements in the inner ring are delayed by a phase shift of kq with respect to those on the outer ring. Such a condition (Eq. (10)) can be easily fulfilled by using a single phase shifter as shown in Fig. 2. This is a simple requirement compared with that needed for a rectangular array of $M \times N$ elements, where $(M \times N)/4$ phase shifters must be used to achieve focusing. Moreover, the above variable phase shifters must be of variable type if a variable focal distance is required. One added advantage of the proposed design is that the compensation in the excitation of the elements for the $1/R$ factor can be easily implemented as there are only two different distances $R1$ and $R2$. Thus, only one magnitude adjustment in the feed network is needed, while in the square array of $N \times N$ elements, there are $N^2/4$ different Rij distances that need to be considered in the magnitude (or $1/Rij$) compensation.

3. COMPUTER SIMULATIONS IN MATLAB

The proposed array was simulated in the MATLAB environment based on the derivations presented in Section 2, where an operating frequency of 2.4 GHz was assumed. The array comprised four elements on the inner ring ($M = 4$), eight elements on the outer ring ($N = 8$), and the radii of the two rings are $a = \lambda = 125$ mm and $b = 3\lambda = 375$ mm, respectively. Therefore, the other parameters will be: $R_1 = 5.099\lambda = 637.4$ mm,
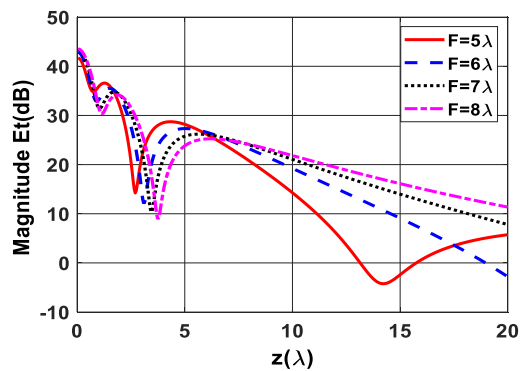
FIGURE 3. Variation of the electric field $E_t(z)$ of the proposed antenna along the normal to the antenna (at the point $P(0,0,z)$) for various values of focal distance F.
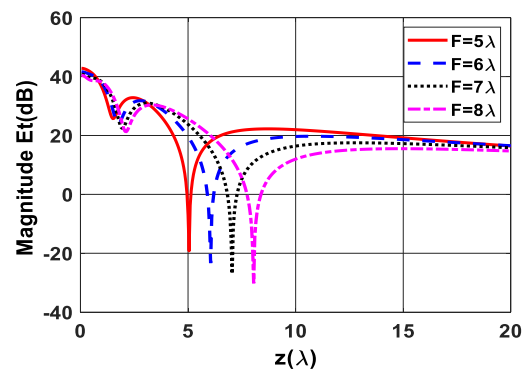

FIGURE 4. Variation of the $E_t(z)$ of the proposed antenna along the normal to the antenna (at the point $P(0,0,z)$) for various values of F, when the added phase shift is $\phi = \pi$.

FIGURE 5. Variation of the $E_t(z)$ of the proposed antenna along the normal to the antenna (at the point $P(0,0,z)$) for various values of F, when the added phase shift is $\phi = \pi/2$.
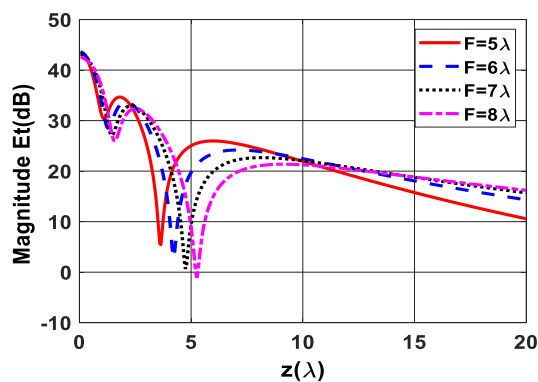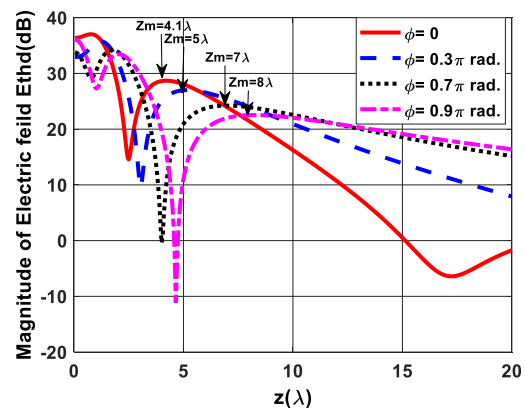

FIGURE 6. Variation of the electric field $E_t(z)$ of the proposed antenna at the point $P(0,0,z)$ for various values of the added phase shift ϕ. ($a = \lambda$, $b = 3\lambda$, and $F = 5\lambda$). The position of the peak value of the field is indicated by Zm.

$R_2 = 5.831\lambda = 728.9\,\text{mm}$, and $\Delta R = R_2 - R_1 = 0.732\lambda = 91.5\,\text{mm}$.

The elements on the inner ring were given excitations magnitude of ($N/M = 2$) that are twice of those on the outer ring so that the two rings have the same contributions at the focal point, as explained in Section 2 (Eqs. (6) & (7)). The obtained results in the form of the variation of the electric field along the normal axis to the array (i.e., along the Z-axis) are shown in Fig. 3 for various design focal distances F. In these simulations, the elements on the inner ring were delayed by (kq) radians for each case of the focal distance F. It can be seen that there is a well-defined focal region with a sharp null at the left of the focus. The focal distance is slightly smaller than the design value F, due to the $1/R$ variation of the electric field radiated from the array elements [1, 10]. Moreover, the peak value of the field at the focus decreased as the design focal distance was increased. The position of the actual focal point shifts away from the array plane as the design value of the focal distance (F) is increased.

To show the effect of the added phase shift (ϕ) that is supplied by the variable phase shifter shown in Fig. 2, the same array was simulated but using a phase shift value of ($\phi = \pi$), and the obtained results are shown in Fig. 4. The figure shows

four cases of the array that was originally designed to have its focus at (5λ, 6λ, 7λ, and 8λ) from the array, and the fixed phase shifter was given the corresponding value of (kq), but the variable phase shifter was set at π radians. Compared to the results of Fig. 3, where $\phi = 0$, it can be seen that there are deep nulls at the positions of the former focal points. This is because the contributions of the two rings are now in opposition rather than in addition due to the added 180° phase of the variable phase shifter. Fig. 5 shows the obtained results when the added phase is $\phi = \pi/2$. It can be observed that the position of the focus was shifted away from the array by about two wavelengths as compared to the results of Fig. 3 where no added phase was used ($\phi = 0$). The shape of the focus is much better than the results of Fig. 4, and the effect of the variable phase shifter has been clearly demonstrated.

For further investigation of the role of the added phase shifter ϕ on shifting the position of the focus, the same array with designed focus at $F = 5\lambda$ was simulated for a number of phase values, and the obtained results are shown in Fig. 6. The results show a smooth movement of the focal point to the right (away from the array) as the phase ϕ is increased. The focus position moved from the point ($z = 4.1\lambda$) to the point ($z = 8\lambda$) by
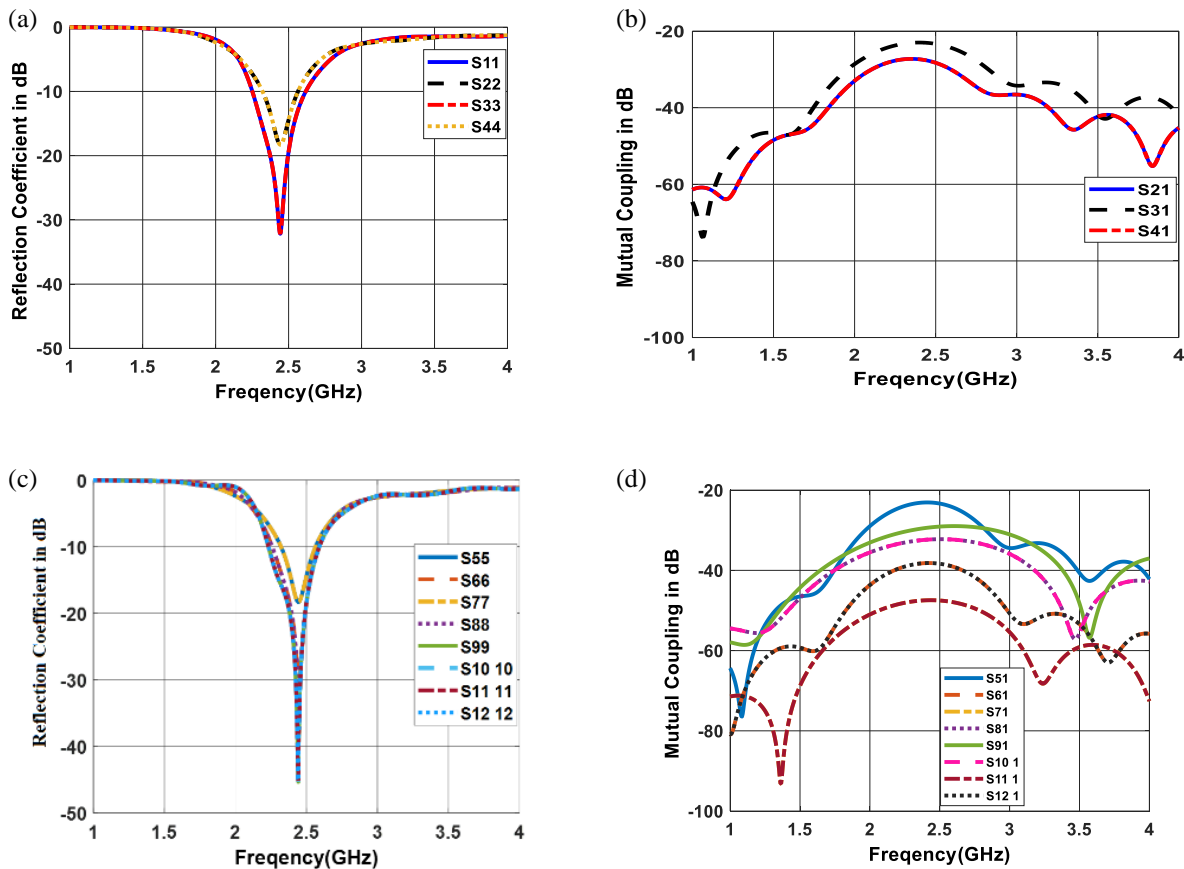
FIGURE 7. Reflection coefficient $|S_{11}|$ and mutual coupling $|S_{ij}|$ versus frequency for: (a), and (b) the inner ring elements, and (c), (d) the outer ring elements.

changing the phase from zero rad to 0.9π rad. It is seen that as the focus is shifted away from the array, the peak value of the field decreases, as it is affected by the $1/R$ propagation factor.

Therefore, the variation of the actual focal length has been achieved by using a single variable phase shifter, which is much easier than the method reported in [19], where the radius of the array has to be adjusted or by changing the thickness of a metallic layer containing the radiating holes as suggested in [21].

3.1. Simulation in the CST Microwave Studio

For further verification of the obtained results from the MATLAB simulations, the same array was simulated in the CST Microwave Studio. To utilize the power of this software, the array elements were assumed to be $\lambda/2$ dipoles that are oriented along the Y-axis. The obtained results for the reflection coefficient at the input of the array elements and the mutual coupling between the elements are shown in Fig. 7 for the two rings. It can be seen that the array elements are matched ($|S_{11}| < 18$ dB) at the design frequency and show a -10 dB bandwidth of 0.27 GHz, which is limited by the bandwidth of the dipole. The elements on the outer ring show a lower reflection coefficient as they are separated by a larger distance than those on the inner ring. The mutual couplings between the elements are lower than -23 dB as a result of the adequate separation of the elements.

The obtained results for the field variation along the normal to the array for three values of the added phase compared to those obtained from the MATLAB simulations are shown in Fig. 8. Very good agreements are noticed for the three cases where the variable phase shifter was set to ($\phi = 0$, $\phi = \pi/2$, and $\phi = \pi$). The small differences in the depths of the nulls can be attributed to the fact that in the MATLAB simulations, isotropic array elements were used, while $\lambda/2$ dipoles were used in the CST simulations. The null to the left of the focus occurs when the contributions of all the elements on the two rings cancel each other. However, the radiation patterns of the elements on the two rings are not exactly the same at the null position, so perfect cancellation was not obtained.

The conventional far-field patterns of the array in the two principal planes were determined by the CST software and are shown in Fig. 9. The patterns are of a broadside type with a defined main beam and surrounding side lobes. The side lobes in the elevation plane (YZ-plane) are lower than those in the horizontal plane (XZ-plane) due to the effect of the dipole elements. The dipoles are oriented vertically, and thus their radiation patterns affect the array pattern in the vertical plane more than in the horizontal plane. The relatively high side lobes can be attributed to the fact that the elements on the inner ring are phase shifted from those on the outer ring for the purpose of near-field focusing. This case is different from the uniform
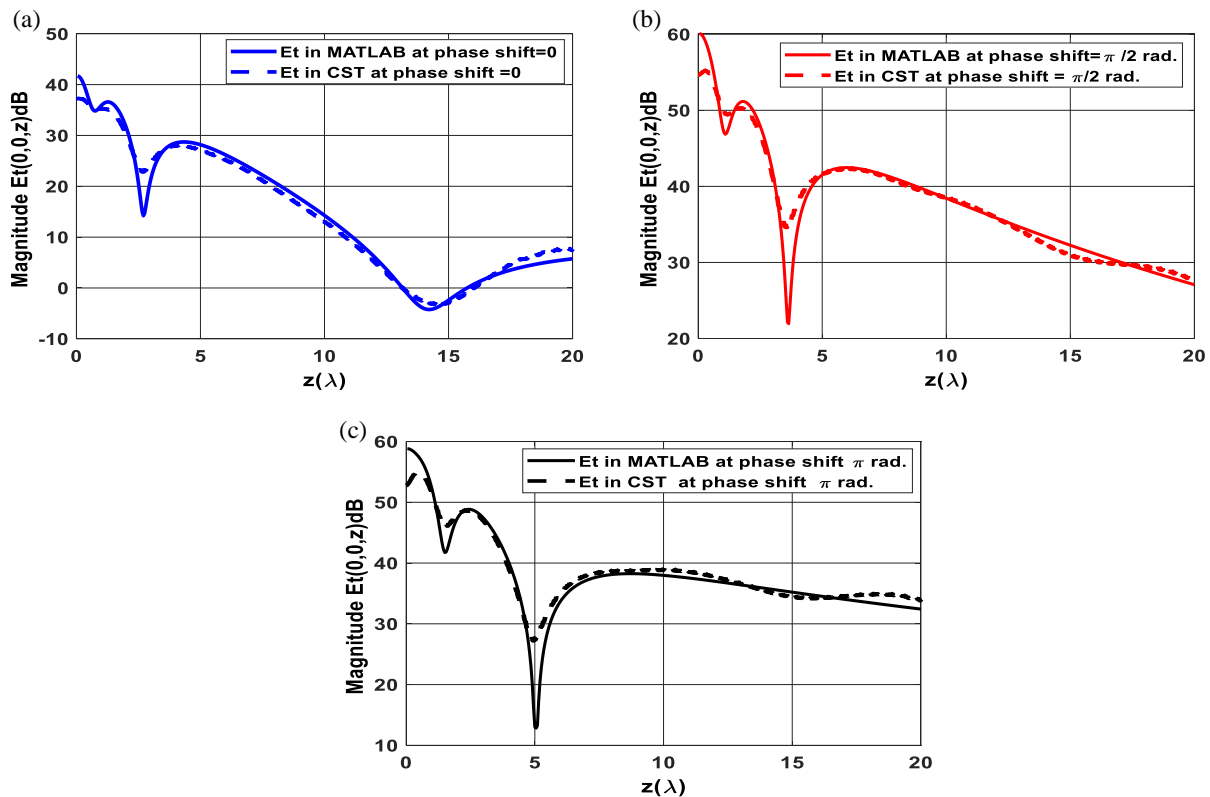
FIGURE 8. Comparison of the variations of the electric field $E_t(z)$ at the observation point $P(0, 0, z)$ obtained from MATLAB and CST simulations. (a) $\phi = 0$, (b) $\phi = \pi/2$, and (c) $\phi = \pi$.
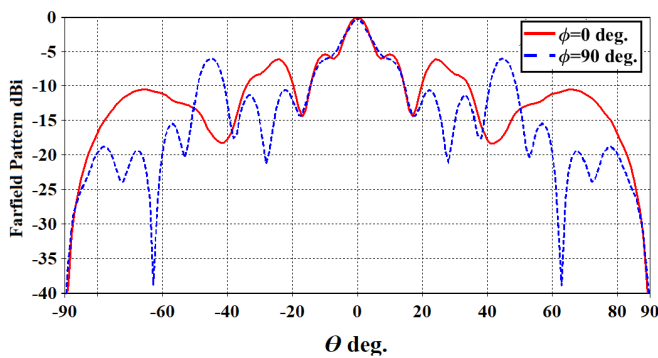

FIGURE 9. Far-field radiation patterns of the proposed array, ($\Phi = 90$) vertical pattern (in the YZ-plane), and ($\Phi = 0$) horizontal pattern (in the XZ-plane).
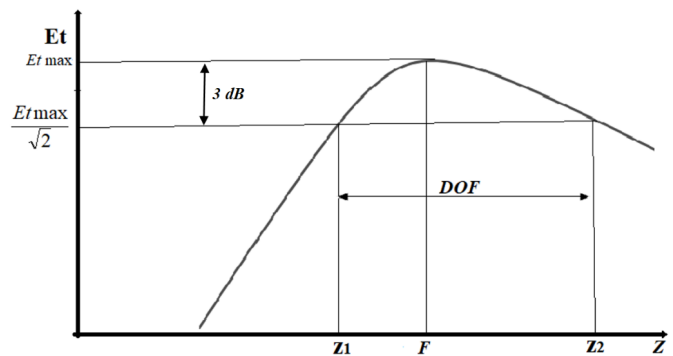

FIGURE 10. Sample of the variation of the electric field along the normal to the antenna (along the Z-axis) around the focus.

planer array where all the elements have the same phase, and the pattern shows a -13 dB side lobe level.

4. ESTIMATION OF THE DEPTH OF FIELD (DOF)

In focused arrays, the radiated field is concentrated at the focal region and eventually decreases as the observation point moves away from the focal point, as shown schematically in Fig. 10. As given by Eq. (10), to achieve a focus at the design focal point $P(0, 0, F)$, the compensation for the path length difference should be ($q = \Delta R = R_2 - R_1$). Therefore, the

radiated field has a maximum value of $2E$, and the field decreases along the points on both sides and away from the focus. The depth of focus or depth of field (DOF) is defined as the distance between the two observation points $P_L(0, 0, Z_1)$ and $P_H(0, 0, Z_2)$, where the field value drops to $1/\sqrt{2}$ of its maximum value. Thus,

$$\text{DOF} = Z_2 - Z_1. \qquad (12)$$

The distances Z_1 and Z_2 can be determined by observing the path length difference ΔR at each of the observation points

TABLE 1. The focal region parameters, and estimated DOF for the array having $a = \lambda$, $b = 3\lambda$, and phase shift $\phi = 0$.

Design focal distance (λ)	Actual focal distance (λ) (MATLAB results)	DOF (λ) (MATLAB results)	Estimated DOF (λ) (formula) (21)
5	4.1	4.6	3.4
6	4.9	5.8	5.2
7	5.5	7	7.5
8	6	8.3	10.6

TABLE 2. Comparison of the parameters of the proposed array with those published in the literature.

	Type of array	Radius (λ) and No. of elements per row	f GHz	No. of Elements	Element type used	Size of array (λ)	Focal length (λ)	DOF (λ)	Focal Spot size (spot width along x-axis) (λ)	Phase shifters
[10]	Square (filled)	$10 * 10$	2.4	100	Isotropic	$4.5*4.5$	5	9.09	0.84	25
	Square ring	25 on square ring	2.4	36	Isotropic	$4.5 * 4.5$	5	101	0.52	9
[17]	Two circular rings	$r1 = 2.4, N1 = 8$ $r2 = 4.8, N1 = 8$	5.8	16	Patch	$Dia = 19.4$	19.3	NA	1.93	1
[18]	Three circular rings	$r1 = 1.9, N1 = 8$ $r2 = 5.8, N2 = 8$ $r3 = 9.6, N3 = 8$	5.8	24	$\lambda/2$ Dipole	$Dia = 19.2$	9.7 / 17.4	1.9 / 5	0.55 / 0.75	2
[3]	Square array	$4 * 4$	10	16	Square patch with U slot	$9.6 * 9.6$	4.2	—	1.6	16
[21]	Square array	$8 * 8$	35	64	Circular aperture	$7.5 * 7.5$	9.8	11	1.16	64
[24]	Square array	$4 * 4$	2.45	16	Patch	$2 * 2$	0.81	1.44	0.72	16
[24]	square array	$6 * 6$	2.45	36	Patch	$3.42 * 3.42$	1.22	1.97	0.7	36
[25]	Square array	$8 * 8$	5.8	64	Dielectric resonator	$5.4 * 5.4$	5.8	5	1.57	64
This work	Dual-ring	$r1 = 1, N1 = 4$ $r2 = 3, N2 = 8$	2.4	12	$\lambda/2$ dipole in CST.	$Dia = 6$	4.1	4.6	0.82	1

$P(0, 0, Z_1)$ and $P(0, 0, Z_2)$ as shown below:

$$\Delta R_{(Z1)} = R_{2L} - R_{1L} = \sqrt{(Z1)^2 + b^2} - \sqrt{(Z1)^2 + a^2} \quad (13)$$

$$\Delta R_{(Z1)} = Z1\sqrt{1 + \left(\frac{b}{Z1}\right)^2} - Z1\sqrt{1 + \left(\frac{a}{Z1}\right)^2} \quad (14)$$

If the array dimensions can allow performing the following approximations:

$$\frac{b}{Z1} \ll 1, \quad \frac{a}{Z1} \ll 1$$

then it can be shown that the path difference from the two rings to the point $P(0, 0, Z_1)$ can be approximated to:

$$\Delta R_{Z1} = \frac{b^2 - a^2}{2Z1} \quad (15)$$

When the observation point is moved from $z = F$ to $z = Z_1$, the path difference increases. When the focusing path length is set as $q = \Delta R$, there is a maximum at the point $z = F$.

$$\because \text{Now if } \Delta R = \frac{\lambda}{4}$$

The total E-field will be

$$E_t = E * e^{-jk(R_1 + q)} \left[1 + e^{-jk(R_2 - R_1)} e^{jkq}\right] \quad (16)$$

As q is the required path difference to get a maximum field at $z = F$, q is chosen such that

$$-k(R_2 - R_1) + kq = 0 \quad \text{or} \quad q = R_2 - R_1 \quad (17)$$

and at this condition

$$|E_t| = 2E$$

However, q is set according to Eq. 8(b), i.e., to focus the array at the point $z = F$. Thus at the observation point $z = Z_1$, the total field will be:

$$E_t = \text{Max}/\sqrt{2} = \frac{2E}{\sqrt{2}} = \sqrt{2}E.$$

At the point $P(0, 0, Z_1)$ or $(z = Z_1)$, the total path difference should be that for the focusing, and an extra value of $\lambda/4$ is needed for the total field to drop to Max/$\sqrt{2}$, or

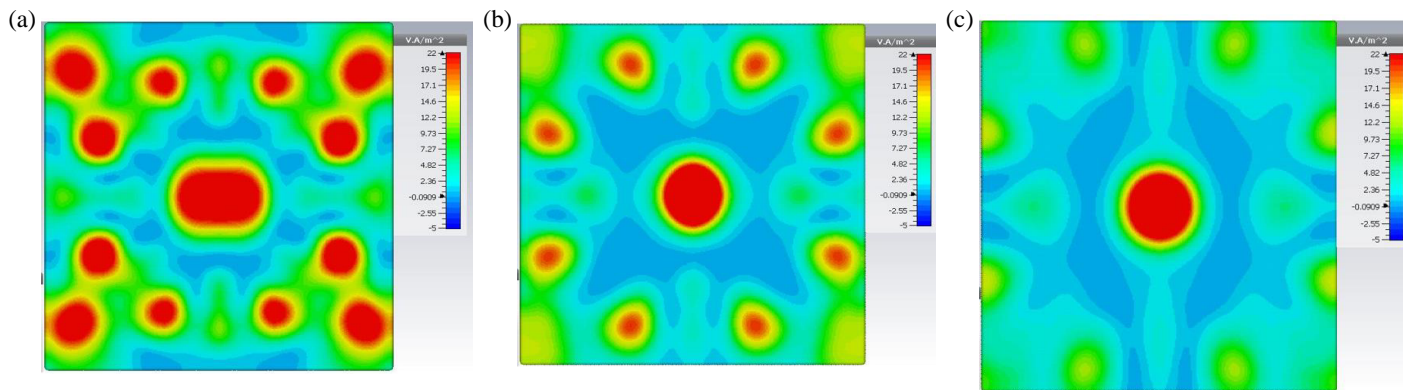$$\frac{b^2 - a^2}{2Z1} = \frac{b^2 - a^2}{2F} + \frac{\lambda}{4} \quad (18)$$

FIGURE 11. Distribution of the power density across the lateral planes passing through the points; (a) $z = 392\,\text{mm}$, (b) $z = 517\,\text{mm}$, and (c) $z = 642\,\text{mm}$ for phase shift $\phi = 0$. The size of the displayed area is $6\lambda \times 6\lambda$.

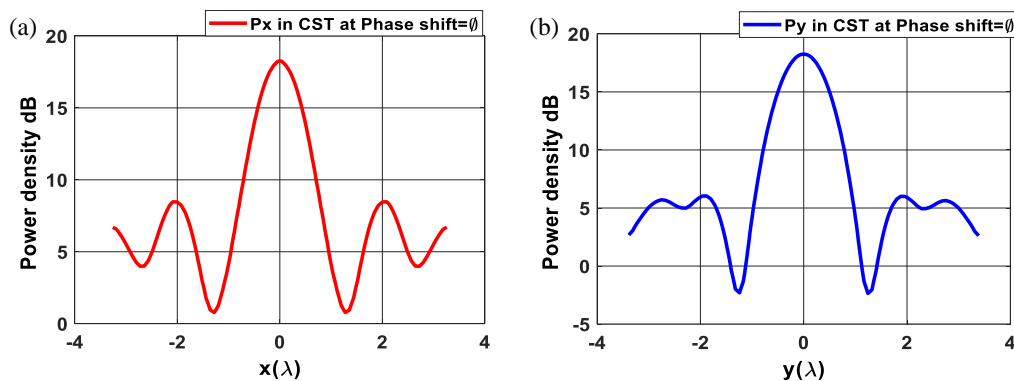**FIGURE 12.** Variation of the power density across the lateral axes on the plane passing through the actual focus ($z = 517\,\text{mm}$), for phase shift $\phi = 0$, $a = \lambda$, $b = 3\lambda$, and $F = 5\lambda$.

which leads to

$$Z_1 = \frac{F(b^2 - a^2)}{(b^2 - a^2) + 0.5\lambda F} \quad (19)$$

Similarly, it can be shown that at the other point ($z = Z_2$), where the total field drops to Maximum/$\sqrt{2}$:

$$Z_2 = \frac{F(b^2 - a^2)}{(b^2 - a^2) - 0.5\lambda F} \quad (20)$$

Then the depth of field is

$$\text{DOF} = Z2 - Z1$$

$$\text{DOF} = \frac{\lambda F^2 (b^2 - a^2)}{(b^2 - a^2)^2 - 0.25\lambda^2 F^2} \quad (21)$$

It should be noted that the above derivation has not considered the $1/R$ conventional decay of the electric field as the observation point moves away from the array.

To test the accuracy of the derived formula for estimating the DOF of the focused array, a number of simulations were performed, and various parameters of the obtained responses were determined. The obtained results are compared in Table 1, which shows that the actual position of the focal point is smaller

than the design value F. This can be attributed to the $1/R$ decay factor, which shifts the point of maximum field towards the antenna. Moreover, the derived formula gives a modest estimate of the DOF, and the actual depth of field is smaller than the estimated value. The reason for this finding is that the derived formula was based on the path length difference only and has not considered the $1/R$ field decay factor.

Another point to notice is that for a given array size (fixed inner and outer radii), as the focal length increases, the depth of field increases. In other words, the focusing capability of the array deteriorates as the focal distance increases, as noticed for focused arrays of rectangular shape [1, 10]. Moreover, the DOF goes to infinity when the focal distance is set at

$$F = \frac{2(b^2 - a^2)}{\lambda} \quad (22)$$

The above relation means that at relatively large distances comparable to the far-filed distance ($2D^2/\lambda$ or $8b^2/\lambda$), the contributions of all array elements are almost in phase, and thus the other point ($z = Z2$) where the field drops to Max/$\sqrt{2}$ cannot be met. Such a feature was also noticed in rectangular arrays [22] where the depth of field is given by the following formula, where the DOF increases with the square of the focal distance.

$$\text{DOF} = 7\lambda(F/2b)^2 \quad (23)$$

5. FIELD DISTRIBUTION ACROSS THE FOCAL PLANE

Of equal importance is the distribution of the focused power density across the focal plane (the plane parallel to the array and passing by the focal point). This distribution shows how the power is confined around the focal point and indicates the success of the focusing process. The array having inner and outer radii of λ and 3λ, respectively, and focused at $F = 5\lambda$ was simulated in CST Microwave Studio, where the array elements were assumed as $\lambda/2$ dipoles. Fig. 11 shows the distribution of the power density across three planes passing through three points that have maximum power density ($z = 517\,\text{mm}$) and those at one wavelength on both sides of the focus, i.e., at ($z = 392\,\text{mm}$ and $z = 642\,\text{mm}$). The field is localized at the center with a circular symmetry due to the circular geometry of the array. It is evident that the best localization of the field is at the actual focal point ($z = 517\,\text{mm}$). However, the field distributions across the planes on both sides of the focal point, which are separated by 2λ (Fig. 11(a), and Fig. 11(c)), still show good focusing. Fig. 12 shows the variation of the power density across the X and Y axes in the plane passing through the actual focus. The plots show a side lobe level of 10.7 dB, a 3 dB lateral width of 103.7 mm along the X-axis, and a side lobe level of 12.2 dB, a 3 dB lateral width of 122.9 mm along the Y-axis. The achieved 3 dB lateral widths of 103.7 mm and 122.9 mm are very close to the value of the wavelength of $\lambda = 125\,\text{mm}$. This result is in line with the formula derived for the lateral width W of the focal spot produced by a focused linear aperture having length L [23]:

$$W = \frac{4\lambda F}{\pi L} \tag{24}$$

For the double circular ring array investigated here ($L = 2b = 6\lambda$ and $F = 5\lambda$), the lateral width according to Eq. (24) can be found to be 1.06λ or 132.5 mm.

However, the obtained value of the depth of field DOF was found to be 4.6λ. These findings are similar to those found in [1, 10] for the rectangular focused array. The slightly wider width and lower side lobe level noticed along the Y-axis is due to the use of the $\lambda/2$ dipole radiating elements that are oriented along the Y-axis. The $\lambda/2$ dipoles produce tapering along the Y-axis, which leads to a lower side lobe level and consequently wider beam.

6. COMPARISON WITH OTHER WORKS

The performance of the proposed antenna is compared with those of published literature as shown in Table 2. The proposed array requires only one variable phase shifter as that of the design in [17], in contrast to the other designs. Therefore, the variable focal distance can be easily obtained from the proposed array and that presented in [17]. While the proposed array has used the smallest number of elements, it has offered a lateral focal spot size of 0.84λ, which is competitive with other designs.

7. CONCLUSIONS

A focused circular array with a focal distance that can be varied by only a single variable phase shifter has been demonstrated. The idea was implemented on a dual-ring circular array having a six wavelength diameter and focused at a five wavelength distance by using a single phase shifter. The theoretical analysis and computer simulations of a sample design using MATLAB and CST Microwave Studio showed that a phase change of 0.9π leads to a four wavelength change in the focal distance along the normal to the array plane. A well-localized focal region about one wavelength in the lateral direction and a few wavelengths in the normal direction to the array was achieved. The derived formula for estimating the DOF showed reasonable accuracy compared to the simulation results. The proposed idea of the circular array is useful and flexible in varying the focal distance by using a single variable phase shifter in contrast to the square array of $N \times N$ elements where $N^2/4$ variable phase shifters are needed to change the focal distance. Moreover, the compensation for the $1/R$ factor can be implemented by a single attenuator at the feed network, in contrast with the square array, where $N^2/4$ compensations are needed. The proposed design can be utilized in hyperthermia, RFID, and imaging applications, where it is required to vary the focal distance by simple electronic means.

REFERENCES

[1] Nepa, P. and A. Buffi, "Near-field focused microwave antennas near-field shaping and implementation," *IEEE Antennas & Propagation Magazine*, Vol. 59, No. 3, 42–53, 2017.

[2] Nepa, P., A. Buffi, A. Michel, and G. Manara, "Technologies for near-field focused microwave antennas," *International Journal of Antennas and Propagation*, Vol. 2017, 17, 2017.

[3] Bogosanovic, M. and A. G. Williamson, "Microstrip antenna array with a beam focused in the near-field zone for application in noncontact microwave industrial inspection," *IEEE Transactions on Instrumentation and Measurement*, Vol. 56, No. 6, 2186–2195, 2007.

[4] Daniels, D. J., *Ground Penetrating Radar*, IET, London, United Kingdom, 2004.

[5] Guo, T. C., W. W. Guo, and L. E. Larsen, "A local field study of a water-immersed microwave antenna array for medical imagery and therapy," *IEEE Transactions on Microwave Theory and Techniques*, Vol. 32, 844–854, 1984.

[6] He, X., W. Geyi, and S. Wang, "Optimal design of focused arrays for microwave-induced hyperthermia," *IET Microwaves, Antennas, and Propagation*, Vol. 9, No. 14, 1605–1611, 2015.

[7] Lee, K., J.-Y. Kim, and S.-H. Son, "Experimental phantom test of 925 MHz microwave energy focusing for non-invasive local thermotherapy," *Results in Physics*, Vol. 38, No. 105585, 2022.

[8] Omrani, A., G. Link, and J. Jelonnek, "A near-field focused phased-array antenna design using the time-reversal concept for weed control purpose," arXiv:2302.01012v1 [eess.SY], Feb. 2, 2023.

[9] Ismail, M. S. and K. H. Sayidmarie, "Investigation of three array geometries for focused array hyperthermia," *The International Symposium on Antennas and Propagation*, Sapporo, Japan, 1992.

[10] Sayidmarie, K. and A. M. Abdulkhaleq, "Investigation of six array geometries for focused array hyperthermia applications," *Progress In Electromagnetics Research M*, Vol. 23, 181–194, 2012.

[11] Tomás, J. J., M. Arrebola, G. León, and F. Las-Heras, "Near-field focussed array with two simultaneous and independent spots," *Proceedings of the 2012 IEEE International Symposium on Antennas and Propagation*, Chicago, IL, USA, 2012.

[12] Yi, X., X. Chen, L. Zhou, and S. Hao, "A high-efficiency near-field focused transmitting antenna based on the equal power divisions," *AIP Advances*, Vol. 10, No. 11, 115111, 2020.

[13] Sayidmarie, K. H. and E. U. Taha, "Development of a semi-circle phased array for local hyperthermia," *2005 IEEE International Symposium on Microwave, Antenna, Propagation and EMC Technologies for Wireless Communications Proceedings*, 1430–1434, 2005.

[14] He, X., W. Geyi, and S. Wang, "A hexagonal focused array for microwave hyperthermia: Optimal design and experiment," *IEEE Antennas and Wireless Propagation Letters*, Vol. 15, 56–59, 2016.

[15] Lyu, C., W. Li, Si Li, Y. Mao, and B. Yang, "Design of ultra-wideband phased array applicator for breast cancer hyperthermia therapy," *Sensors*, Vol. 23, 1051, 2023, https://doi.org/10.3390/s23031051.

[16] Yildiz, G., I. Farhat, L. Farrugia, J. Bonello, K. Zarb-Adami, C. V. Sammut, T. Yilmaz, and I. Akduman, "Comparison of microwave hyperthermia applicator designs with fora dipole and connected array," *Sensors*, Vol. 23, 6592, 2023, https://doi.org/10.3390/s23146592.

[17] Siragusa, R., P. Lemaitre-Auger, and S. Tedjini, "Near field focusing circular microstrip antenna array for RFID applications," *IEEE Antennas and Propagation Society International Symposium*, 1–4, 2009.

[18] Siragusa, R., P. Lemaitre-Auger, and S. Tedjini, "Tunable near-field focused circular phase-array antenna for 5.8-GHz RFID applications," *IEEE Antennas and Wireless Propagation Letters*, Vol. 10, 33–36, 2011.

[19] Huang, R., B. Liu, and Q. Tan, "A near-field focused circular array based on dielectric resonator antenna," *IEEE International Symposium on Antennas and Propagation and USNC-URSI Radio Science Meeting (APS/URSI)*, Dec. 4–10, 2021.

[20] Fwzi, M. Z. M. and K. Sayidmarie, "A circular array with improved focusing properties," *Progress In Electromagnetics Research C*, Vol. 126, 13–22, 2022.

[21] Cheng, Y. J. and F. Xue, "Ka-band near-field-focused array antenna with variable focal point," *IEEE Transactions on Antennas and Propagation*, Vol. 64, No. 5, 1725–1732, May 2016.

[22] Graham, W. J., "Analysis and synthesis of axial field patterns of focused apertures," *IEEE Transaction on Antennas and Propagation*, Vol. 31, No. 4, Jul. 1983.

[23] Smith, D., V. Gowda, O. Yurduseven, S. Larouche, G. Lipworth, Y. Urzhumov, and M. Reynolds, "An analysis of beamed wireless power transfer in the fresnel zone using a dynamic, metasurface aperture," *Journal of Applied Physics*, Vol. 121, 014901, 2017, http://dx.doi.org/10.1063/1.4973345.

[24] Shan, L. and W. Geyi, "Optimal design of focused antenna arrays," *IEEE Transactions on Antennas and Propagation*, Vol. 62, No. 11, 5565–5571, Nov. 2014.

[25] Zainud-Deen, S. H., H. A. Malhat, and K. H. Awadalla, "Dielectric resonator antenna phased array for fixed RFID reader in near field region," *Proceedings of the Japan-Egypt Conference on Electronics, Communications and Computers Conference (JEC-ECC'12)*, 102–107, Alexandria, Egypt, Mar. 2012.